Soft Matter

PAPER

View Article Online
View Journal | View Issue

Cite this: *Soft Matter*, 2016, 12, 7855

Received 2nd May 2016,
Accepted 17th August 2016

DOI: 10.1039/c6sm01011c

www.rsc.org/softmatter

Spontaneous exfoliation of a drying gel†

Jun Young Chung,‡[ab] Ido Regev‡[ac] and L. Mahadevan*[abd]

Wet starch cracks when it dries inhomogeneously, while hot glass cracks when it cools non-uniformly. In both cases, differential shrinkage induced by drying/cooling from the surface causes superficial cracks to grow perpendicular to the surface in different patterns. In contrast with these observations of bulk cracking in brittle materials, when a soft and homogeneously swollen polymer gel dries, differential strains lead to the peeling of a thin layer that spontaneously tears away from the bulk. Continued drying leads to the process repeating itself, forming a peeled-layered structure. The emergent thickness of the exfoliated layer is a function of both the geometry of the original gel and the physical parameters associated with the drying rate and external temperature. We characterize the experimental conditions under which layer peeling can arise, and use simulations to corroborate these observations. Finally, a minimal theory explains the scaling of the peel thickness, consistent with our experiments.

Introduction

Non-uniform shrinkage in drying porous media is of much interest in various fields including soil science,[1,2] food processing,[3] materials physics and engineering,[4,5] as well as art conservation.[6] This has led to considerable progress in understanding the dynamics of drying in relatively brittle solids like soils, rocks, and ceramics,[7–11] with the aim of creating strategies for its control and utilization. Since loss of moisture first occurs at the surface, a drying front forms there and propagates inwards, separating the dry or partially dry areas from completely wet areas. As the disordered liquid front separating the wet and dry regions moves, the large capillary stresses across the meniscus in the porous medium cause the solid to shrink inhomogeneously. This leads to a strain gradient with concomitant tensile residual stresses within the material that leads to cracking along the drying direction in brittle materials[12–16] and buckling in low-dimensional soft systems, such as polymer and gel shells.[17–19] In this study, we show that drying-induced differential shrinkage in bulk polymers and gels can exhibit an unusual phenomenon of periodic exfoliation of layers as the rate of drying is increased (Fig. 1A–D).

The observed phenomenon is reminiscent of the curling of dessication-cracked polygons in sediments[20,21] and thermal delamination in layered materials,[22,23] but it differs in that it does not require or assume a layered or heterogeneous structure. Instead, it arises because of the dynamical processes at work. Earlier theoretical approaches, *e.g.*, ref. 24, describe mud peeling in drying soils by adapting an earlier model for thermal shock spalling.[25] These models provide valuable insights into the mechanism of peel formation, but they are idealized and lack direct experimental confirmation in a controlled laboratory setting. Here, we explore and characterize the phenomenon of spontaneous exfoliation of a drying gel using controlled laboratory experiments, which we then proceed to explain using a combination of theoretical and numerical approaches that emphasize the role of the toughness gradient and inhomogeneous drying.

Results

Our model system consists of a soft, lightly cross-linked poly(dimethylsiloxane) (PDMS) network that is highly and homogeneously swollen with hexanes (see the Materials and methods section). Swollen gels were dried under controlled temperature conditions to adjust the evaporation rate. As shown in Fig. 1A and B, we find that when subjected to relatively high temperature drying conditions, the swollen gel shrinks upon drying and develops cracks on the surface. As the drying process proceeds, the cracks penetrate into the bulk, but upon reaching a certain depth a layer exfoliates spontaneously (Fig. 1C). After the first layer peels off, the initial crack progresses further into the bulk until at a certain depth a second layer peels away (Fig. 1D).

[a] *Paulson School of Engineering and Applied Sciences, Harvard University, Cambridge, MA 02138, USA. E-mail: lm@seas.harvard.edu*
[b] *Wyss Institute for Biologically Inspired Engineering, Harvard University, Cambridge, MA 02138, USA*
[c] *French Associates Institute for Agriculture and Biotechnology of Drylands, Jacob Blaustein Institutes for Desert Research, Ben-Gurion University, Sde Boker Campus, 84990, Israel*
[d] *Department of Physics, Harvard University, Cambridge, MA 02138, USA*
† Electronic supplementary information (ESI) available. See DOI: 10.1039/c6sm01011c
‡ These authors contributed equally to this work.

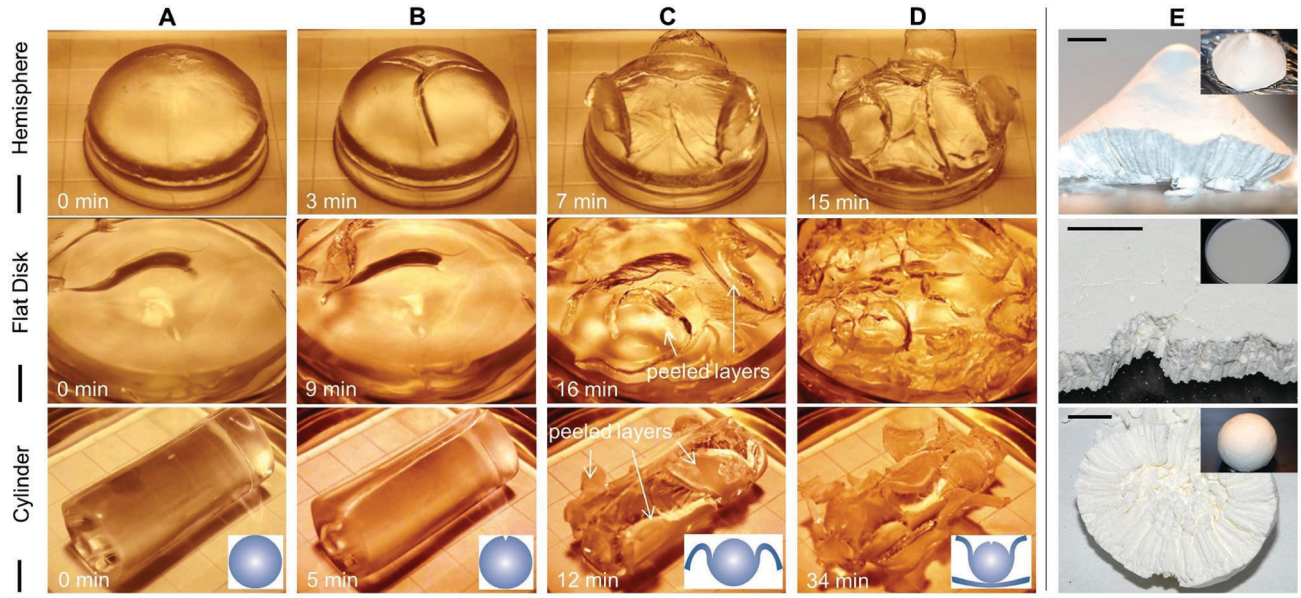

Fig. 1 Recurrent spontaneous exfoliation of a drying solvent-infused cross-linked gel, contrasted with cracking of drying wet starch. (A) Initial swollen state of gels (cross-liked PDMS network in hexanes) with different geometries before drying (scale bars = 10 mm). (B) Formation of visible cracks on the surface caused by the shrinkage of the gel upon drying at elevated temperatures ($T > 40$ °C), which propagate inwards into the bulk as the drying progresses. Note that these cracks occur at random locations on the surface (for comparison, see Fig. S1, ESI†). We believe that the presence of defects or impurities on the samples is an unavoidable reality and these kinds of weak points are most probably the loci for crack initiation. (C) Subsequent peeling off of a thin superficial layer (O(mm) thick), exposing the bare surface of the underlying gel. (D) Repeated cycle of cracking and peeling, which recurs several times until the gel is completely dried. (E) Crack patterns formed by drying a starch slurry (scale bars = 10 mm; insets: the original sample geometry before drying). Experiments were performed in mixture of cornstarch (Argo) and water under the similar drying conditions as for the gel, and the desiccated samples were carefully split to reveal their internal structure.

This scenario repeats itself until the gel completely dries out (Movie S1, ESI†). We observe the same qualitative behavior regardless of whether the sample surface is flat, singly-curved as in a cylinder, or doubly-curved as in a hemisphere (Fig. 1A–D). Observations of the process also reveal that the peeled layer initially curls upwards away from the newly exposed surface and then slowly returns back down to the surface as the drying progresses (Movie S1, ESI†). This implies the existence of a strain gradient in the radial (or thickness) direction and furthermore that this gradient diminishes as the whole peeled layer dries out, similar to the curling behavior of a paper strip when in contact with water/moisture from one face.[26–28] It is useful to contrast these behaviors with those observed in the drying of brittle materials, such as granular or poorly consolidated porous media, which exhibit vertical cracking/splitting.[8,11–13] As an example, we present in Fig. 1E the results obtained for starch slurries with different geometries. A mixture of starch and water cracks as it dries out and forms a polygonal array of closely packed columns that run perpendicular to its topographic surface, independent of whether the surface is flat or curved, and further shows no additional relaxation as the crack progresses deeper into the bulk. Thus, we can rule out curvature as the primary cause for the observed exfoliation instability of a drying gel.

To quantify the conditions for occurrence of the exfoliation instability and the emergent thickness of the resulting peeled layer, we first studied the effects of changing the environment (temperature) and of the size, shape and composition of the sample and the wind speed on cracking and peeling (see the Materials and methods section). To assess the dependence on drying temperature in a systematic manner, we conduct a set of experiments in which long cylindrical gels are dried in air under different temperatures T. At room temperature or slightly above it, we find that the gels deswell gradually without any cracking or peeling (Fig. 2A, black and blue curves; also see Movie S2, ESI†). When dried above a critical temperature, in this case $T_c \approx 40$ °C, the gels undergo repeated cycles of cracking and peeling, and the rate of solvent removal is even faster at higher temperatures (Fig. 2A, green and red curves; also see Movie S3, ESI†). The signature of the peeling events manifests itself as jumps in the rate of solvent loss as a function of time (arrowheads in Fig. 2A), associated with exposing a new surface.

To explain when and how the exfoliation arises, we first note that the drying of gels involves several stages.[3,4] In the initial phase, liquid is lost primarily from the surface and the rate of drying is constant in time; this does not cause any strain gradients in the material. However, as the drying continues, the liquid at the surface is depleted to such an extent that the capillary menisci deform and start to recede into the bulk, concomitant with appearance and propagation of a drying front into the interior of the solid network.[9,10] Simultaneously, the drying solid starts to shrink in response to the loss of fluid and the meniscal capillary forces at the interface. Across this relatively sharp drying front there is a volumetric strain gradient that leads to tension in the outer layer that is prevented from

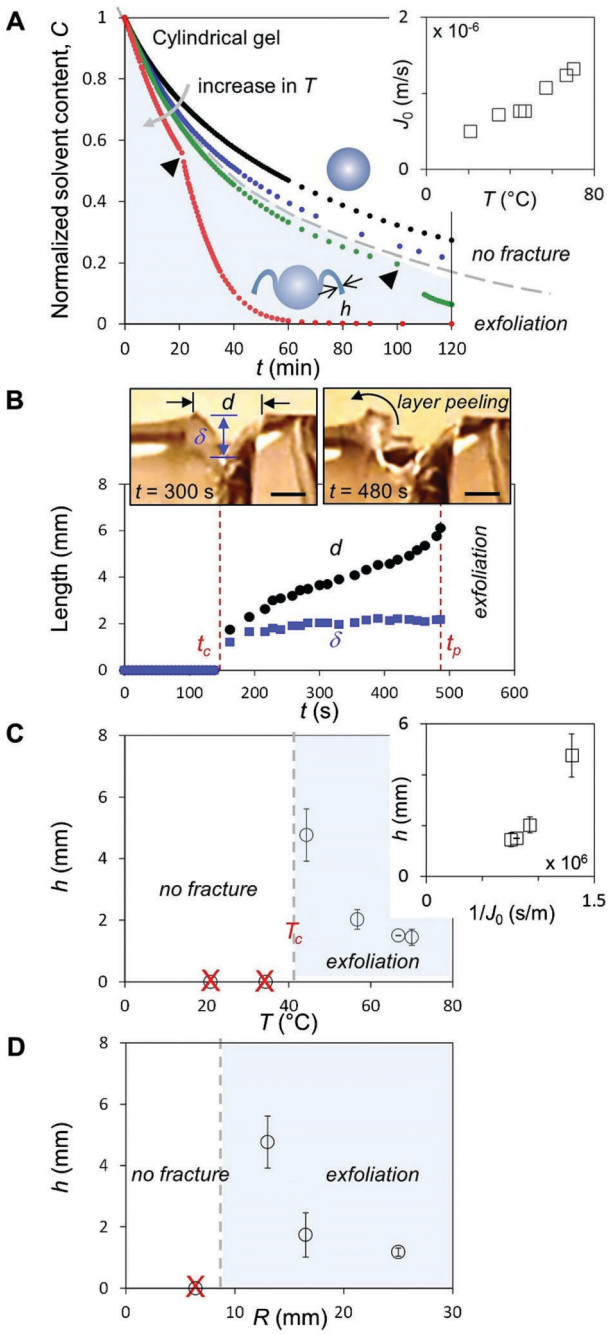

Fig. 2 Drying of swollen cylindrical gels by the evaporation of solvent at elevated temperatures. (A) Normalized solvent content of gels, $C(t) = (m_0 - m(t))/(m_0 - m_\infty)$, as a function of drying time t for different drying temperatures (T = 21, 34, 45, and 57 °C for black, blue, green, and red circles), where m_0 and m_∞ are the initial (fully swollen) and final (fully dried) sample weights. The dashed gray line marks the transition between the deswelling without fracture and the layer exfoliation (blue background). The kinks, marked by arrowheads, indicate the onset of exfoliation. Inset: Initial evaporation flux, $J_0 = (dm_0/dt)/\rho_s S_0$, plotted against T, where dm_0/dt is the initial solvent evaporation rate, ρ_s is the solvent density, and $S_0 = \pi R^2 L$, which is the initial surface area of the swollen cylindrical gel (initial radius $R \approx 13$ mm and length $L \approx 63$ mm). (B) Crack opening displacement d and penetration depth δ at different times (t_c and t_p are the time at the initiation of cracking and peeling, respectively; scale bars = 2 mm). (C) Thickness of the first exfoliated layer h plotted against T. Inset: Plot of h *versus* $1/J_0$. (D) Dependence of h on R at T = 45 °C. The red "X" marks in (C) and (D) denote that the gels shrink without fracture. Error bars show standard deviations.

shrinking by the inner swollen core that is put into compression. When the strain in the superficial layer is larger than a critical value, this can trigger sub-critical crack propagation into the bulk of the solid.[11,14]

In contrast, many poorly consolidated solids – particularly starch materials[15,29] – tend to form vertical cracks or columnar joints when dried but do not peel, as shown in Fig. 1E. It is important to note that normal cracks allow for relief of tangential strain, while tangential cracks and layer bending allow for relief of normal strains. The pore sizes of starch are typically on the order of $\ell_p \sim 10^{-6}$ m (ref. 30), orders of magnitude larger than any molecular dimensions, and consequently the migration of fluids (water) through the porous network occurs predominantly by advection. Thus, drying is relatively fast and complete by the time the solid cracks. However, in the soft, highly deformable, cross-linked gel system considered here, the pore size or the mesh size of the swollen network is about two orders of magnitude smaller ($\ell_p \approx 1 \times 10^{-8}$ m; see the Materials and methods section) and is significantly reduced in the course of drying, and only a few times molecular dimensions (≈6 Å for hexanes). In this case, drying is expected to be eventually diffusion-limited, and is thus not completed by the time the vertical cracks first arise. Thus, tensile strain continues to build up in the upper layer even after the vertical crack has formed and stops as the tip moves into the much tougher partially dry or wet region. The increase in toughness is because the solid is less strained due to the local redistribution of solvent[31,32] and is peculiar to soft gels. The time associated with crack growth retardation, or the characteristic time for poroelastic solvent migration,[32] scales as $\tau_p \sim \delta^2/D_p$, where δ is the crack length and $D_p \sim \ell_p^2 E/\mu$ (E being the drained elastic modulus of the gel, and μ being the solvent viscosity) is the effective poroelastic diffusivity, which can and does change during the course of drying as E increases and ℓ_p decreases. Drying along the crack face, together with the vertical strain gradient in the uncracked solid, leads to a peeling torque in the neighborhood of the crack. If the strains build up sufficiently before the crack grows inwards to catch up with the advancing drying front,[14] a lateral crack will nucleate which will cause the upper layer to peel away. Once this happens there is a new exposed surface of wet material and the same process can repeat itself.

In Fig. 2B, we show how slow drying changes the dynamics of strain buildup and release. Once the surface strain becomes large enough to nucleate a crack from a critical flaw, a crack initiates at the surface ($t = t_c$) and propagates rapidly to a certain depth δ, and then remains stationary owing to the increased toughness of the wet gel ahead of it. During this time, the crack opening displacement d continues to increase and hence the strain gradient through the upper layer thickness increases, causing the buildup of a curling torque. In the presence of a strong radial fracture toughness gradient, the crack cannot yet propagate radially, and instead turns allowing a layer to exfoliate and curl up ($t = t_p$). Using an estimate of $D_p \approx 10^{-8}$ m^2 s^{-1} (see the Materials and methods section), we find the time for poroelastic relaxation over $\delta \approx 2$ mm to be $\tau_p \approx 400$ s, which is comparable to the time before the

peeling of a layer $\tau(=t_p - t_c) \approx 350$ s. In contrast, for starch, $D_p \approx 10^{-5}$ m^2 s^{-1} (ref. 15), and the poroelastic relaxation time $\tau_p \approx 0.4$ s, so that unconsolidated materials respond much faster to drying than cross-linked gels. These estimates confirm that exfoliation in consolidated clays or soft cross-linked gels is driven by the combination of accumulated strain due to shrinkage that is accompanied by slow solvent flow and crack growth retardation in a toughness gradient. This is in contrast with the case of a strain gradient alone that will only cause the crack to propagate radially. Since crack retardation and the continuous opening of the crack are particular to soft gels, this explains how a uniform gel can peel. We should point out that although the peeling seen in homogeneously structured gels is similar to that causing mud curling, in the latter, the strain gradient is commonly associated with a textural heterogeneity,[20,21] since clay platelets are packed differently near the surface. It is also important to emphasize that the thickness of the peeled layer emerges from the coupled dynamics of drying and fracture, unlike in classical thin film fracture[25] where the thin film delaminates or peels away at the interface.

To characterize the mechanisms that control this emergent length scale, we vary the drying temperature and thence the evaporative flux as well as the radius of the drying gel, which together control the strain gradient induced by drying, limiting ourselves to the case of cylinders initially. Using the data in Fig. 2A for the mass of the gel (or equivalently the solvent) as a function of time for a given drying temperature, we calculate the initial evaporation flux J_0 as a function of the drying temperature T, as shown in the inset to Fig. 2A. In Fig. 2C, we see that the thickness of the first exfoliated layer h decreases as T is increased, and below a critical drying temperature $T_c \approx 40$ °C (or equivalently below a critical evaporation flux $J_{0c} \approx 7 \times 10^{-7}$ m s^{-1}), there is no exfoliation. In the inset to Fig. 2C, we see that for values of J_0 above the threshold, h increases monotonically with $1/J_0$. In Fig. 2D, we show the thickness of the peeled layer as a function of the initial radius of the swollen gel R, and see that as R is increased, h decreases.

To quantitatively understand these results, we need to characterize the dynamics of the drying front, and couple it to criteria for the fracture of the gel. The former sets the size of the strain gradient which is present over a scale comparable to the width of the drying front w; when it is large, the gradient is small. The front width is known to depend on the front velocity,[33,34] which in turn is directly related to the evaporative flux. Thus, qualitatively, we can expect that when the front width w is very diffuse, the strain gradient will not be strong enough to induce peeling. On the other hand, as the drying rate is increased, the front localizes which increases the strain gradient, leading to peeling. We now turn first to a numerical characterization of this dynamical process and then use scaling and continuum approaches to explain the results.

Numerical simulations

To understand the relative roles of strain and fracture toughness gradients in cracking and peeling, we model the drying cylindrical gel in plane strain using a system of particles arranged in a disc, and connected *via* linear springs to six neighbors in a hexagonal lattice. We assume that each particle follows overdamped dynamics, so that:

$$\xi \frac{\partial \mathbf{r}_i}{\partial t} = \sum_{j \in N_i} \mathcal{K}\left(|\mathbf{r}_i - \mathbf{r}_j| - d_{ij}\right), \tag{1}$$

where ξ is the friction coefficient, $\mathcal{K}$ is the spring constant, and $\mathbf{r}_i$ and $\mathbf{r}_j$ are the positions of neighboring particles labeled i and j, respectively, and separated by a natural rest length d_{ij}, N_i being the set of neighbors of i. The strain gradient induced by drying from the surface is modeled by decreasing the rest length d_{ij} between the particles as a function of space and time, in both tangential and radial directions, that leads to a strain incompatibility between the different concentric layers.

In order to allow fracture we introduce a criterion for bond breaking. If the distance between the particles increases beyond a critical threshold value,

$$|\mathbf{r}_i - \mathbf{r}_j| > \Gamma(r_i,t) d_{ij}(r_i,t), \tag{2}$$

the bond will be broken and the particles will not be linked by a spring. The function $\Gamma(r_i,t)$ characterizes the spring toughness which allows for a differential resistance to fracture, or fracture toughness.

As mentioned above, we expect that interfacial tension will cause the boundary between the wet and dry regions to be relatively sharp, and induce a large volumetric strain due to the change in the water content between the wet and dry regions. In order to model these effects, the space-time dependence of d_{ij} is assumed to be of the form associated with a moving strain front:

$$\frac{d_{ij}(r_i,t)}{d_w} = 1 - \alpha(t)\left[1 + \tanh\left(\frac{r_i - R + v_f t}{w}\right)\right], \tag{3}$$

where d_w is the undeformed spring length at $t = 0$ corresponding to the initial swollen state, R is the cylinder radius, v_f is the front velocity, and w is the front width. $\alpha(t)$ accounts for early stage drying shrinkage, which is assumed to have a simple linear form $\alpha(t) = \alpha_0 t$ until the time t reaches a predefined value τ. The tensile strain $\varepsilon(r_i,t)$ produced in the network is defined as $\varepsilon = 1 - d_{ij}/d_w$. The space-time dependence of Γ is associated with the fact that moisture content changes the toughness. We model this with a toughness profile which will have the same width w and front velocity v_f as the strain profile, since both are caused by drying, and assume the form:

$$\frac{\Gamma(r_i,t)}{\Gamma_w} = 1 - \alpha(t)\left[1 + \tanh\left(\frac{r_i - R + v_f t}{w}\right)\right], \tag{4}$$

where Γ_w is the spring toughness in the wet area.

In our simulations, we vary the front width w, and hence the strain and toughness profiles [eqn (3) and (4), respectively], to explore its effect on crack propagation. We find that when w is large relative to the size of the system, the preexisting crack does not grow at all. As w becomes comparable to or smaller than the size (radius) of the gel, the crack propagates inwards but eventually it stops (Fig. 3A), and when w becomes much

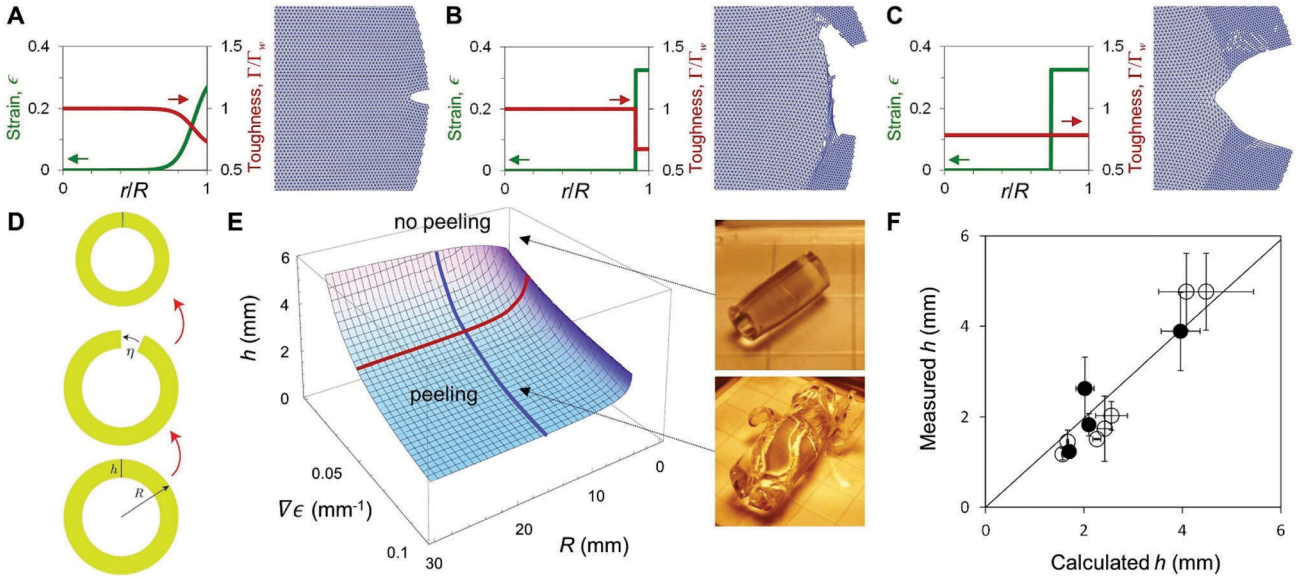

Fig. 3 Numerical simulations and theoretical prediction. (A–C) Simulations of circular elastic networks with a notch that are subject to strain and/or toughness gradients, representing the effect of the drying front on a cylindrical gel: (A) when the drying front is wide ($w = 10$), there is no peeling; (B) for a sharp front ($w = 5 \times 10^{-4}$), the crack propagates radially for some distance and then starts to peel. In both cases, all other parameters are identical (see the Materials and methods section for details on parameter values), and the results for two intermediate values of w are shown in Fig. S2, ESI;† (C) when the toughness is held constant while keeping all other parameters same as in (B), the crack keeps propagating inwards into the bulk (see also Fig. S3, ESI† for simulations with different values of w). (D) Schematic of the theoretical model, from bottom to top: the cylinder circumference is scaled by a factor $1/\eta$, displacement is applied in order to preserve continuity and the configuration is relaxed to the equilibrium (zero forces) configuration. (E) Analytical solutions for the peeled layer thickness h as a function of the strain gradient $\nabla\varepsilon$ and cylinder radius R with $\Gamma/E = 0.25 \times 10^{-4}$ m, where Γ and E are the fracture toughness and elastic modulus of the gel, respectively. Insets: Experimental images representing peeling and no-peeling case. (F) Comparison of the experimentally determined layer thicknesses h with those calculated from the theory. Open and filled circles correspond to the experiments shown in Fig. 2 and Fig. S4, ESI,† respectively. Error bars show standard deviations.

smaller than the system size (corresponding to sharp strain and toughness gradients) the crack propagates a certain distance through the gel and then begins to peel (Fig. 3B). These results indicate that although the tangential strain increases due to drying, it is relieved initially by radial cracking. However, the increase in the toughness gradient as one moves into the wet sub-layer prevents the crack from continually growing radially. Instead the radial strain gradient leads to the peeling of a layer as the preferred mode of strain energy release. However, when the toughness gradient is small or absent (*i.e.*, Γ being held constant rather than having the form given in (4)), the crack propagates radially without changing its direction (Fig. 3C). All together, our numerical results show that we need both a sharp strain gradient together with a large toughness gradient to induce layer exfoliation.

Continuum theory

Having shown that our numerical simulations confirm the basic mechanism for spontaneous exfoliation, we now turn to a continuum approach to the problem. If the strain gradient in a bulk solid with a flat surface scales as $\nabla\varepsilon$, and h is the (unknown) length scale over which the gel moisture content varies, the stored energy per unit width of the solid scales as $E(h\nabla\varepsilon)^2 h\ell$, where E is the elastic modulus of the gel and ℓ is the putative lateral crack length. Balancing this bulk energy with the surface energy associated with the opening of crack that scales as $\Gamma\ell$, we find that the characteristic thickness of the peeled layer scales as $h \sim (\Gamma/E(\nabla\varepsilon)^2)^{1/3}$. As a rough approximation, if we assume a steady rate of evaporation J_0 and linear poroelaticity, Darcy's law implies that the strain gradient $\nabla\varepsilon \sim J_0\mu/E\kappa$, where μ is the dynamic viscosity of the solvent and κ is permeability. This relation then implies that $h \sim [(\Gamma E)^{1/2}\kappa/J_0\mu]^{2/3}$, as derived in ref. 24.

If the surface of the solid is curved, we expect to have the same elastic energy up to corrections of the order of h/R. To see this, we note that for a cylinder of radius R, assuming plane strain in polar coordinates, we find that the strain components may be written as:[35] $\varepsilon_{\rho\rho} = \mathrm{d}r(\rho)/\mathrm{d}\rho - 1$, $\varepsilon_{\phi\phi} = (r/\rho)\eta - 1$, and $\varepsilon_{\zeta\zeta} = 0$, where $r(\rho)$ is the current (deformed) radius that was originally at a location ρ, the material coordinate, and η is the tangential stretch (see Fig. 3D). For small deformations $r \sim \rho$, we may write $\varepsilon_{\phi\phi} \sim \eta - 1$. The strain energy released by a crack of length ℓ will therefore be:

$$\mathscr{U} = E\int_0^{\ell/R}\int_{R-2h}^{R}(\eta-1)^2 r\,\mathrm{d}r\,\mathrm{d}\theta, \tag{5}$$

which on integrating yields:

$$\mathscr{U} = E\ell(\eta-1)^2 h\left(1-\frac{h}{R}\right). \tag{6}$$

Balancing this energy with the fracture energy Γ to open a lateral crack (peel) of length ℓ and substituting an approximate

expression for the strain gradient $\nabla\varepsilon \sim (\eta - 1)/2h$, we obtain the condition for peeling as:

$$h^3\left(1 - \frac{h}{R}\right) \sim \frac{\Gamma}{E(\nabla\varepsilon)^2}. \quad (7)$$

In Fig. 3E, we plot the solution for h against the parameters $\nabla\varepsilon$ and R for a fixed value of Γ/E, and see that h decreases as $\nabla\varepsilon$ and R increase, consistent with our experimental observations. In the limit of very small strain gradients, with $\nabla\varepsilon \to 0$ (small J_0), we find that $h \to \infty$ and since h cannot be larger than R, peeling will not occur. We find that a nontrivial solution to eqn (7) exists only when $\nabla\varepsilon \geq \nabla\varepsilon_c \sim (\Gamma/ER^3)^{1/2}$; thus, there is a threshold level of strain gradient $\nabla\varepsilon_c$ (hence J_{0c}) required for the onset of exfoliation. This is indeed found to be the case experimentally (see Fig. 2A). For a flat surface with semi-infinite thickness ($R \to \infty$), h has a finite limit given by $h \sim (\Gamma/E(\nabla\varepsilon)^2)^{1/3}$, consistent with our previous scaling estimate. We see that the thickness depends only on the stiffness, toughness, and strain gradient and explains why peeling can occur even in a flat geometry (see Fig. 1, middle panels).

A direct comparison of our experimental results with our theoretical estimates requires knowledge of R, Γ/E, and $\nabla\varepsilon$. We choose $\Gamma/E \sim 1 \times 10^{-4}$ m as a typical value reported in the literature for lightly cross-linked PDMS networks,[36,37] and obtain estimates of $\nabla\varepsilon$ separately for each set of experiments by considering the crack opening shape (see the Materials and methods section). Using these estimated values together with the known value of R, we deduce the layer thickness h from the following expression: $h^3(1 - h/R) \sim c\Gamma/E(\nabla\varepsilon)^2$, where c is a constant of proportionality. Comparing these calculated h with our experimentally determined values, we find that the two values agree fairly well for a value of $c \approx 0.2$ (Fig. 3F).

Discussion

Cracking and delamination occur in nonequilibrium processes (for instance, rapid cooling or solidification) which lead to the formation of spatially non-uniform residual stresses developed from a homogeneous state.[38–40] Here, we have uncovered a variation of a fracture instability in a rapidly drying gel that leads to an iterated series of spontaneous exfoliating layers. Notably, this instability does not arise due to preexisting inhomogeneities in the material (*e.g.*, sediment grain-size gradient as in ref. 20), but due to the emergence of a dynamical length scale as a result of the drying process, and is thus different from the typical interfacial cracking or delamination observed in layered materials,[22,23,25] where the layer thickness is prescribed. Using numerical simulations, we have shown that the occurrence of peeling is due to the existence of both shrinkage and toughness gradients generated by the dynamics of drying. Our results show that the peel thickness depends on the strength of the gel network, sample geometry, and the strain gradient associated with drying shrinkage, and can be explained using a minimal theoretical model.

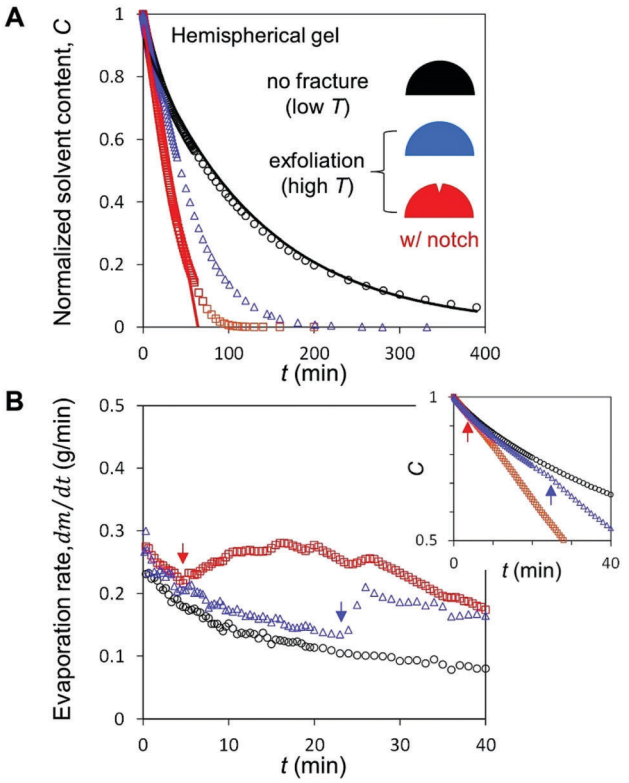

Fig. 4 Control of solvent release by exfoliation instability. (A) Normalized solvent content C of hemispherical gels as a function of drying time t: black circles and blue triangles are for samples with the same initial geometry but at different temperatures (T = 21 and 45 °C, respectively), where the blue triangles show faster evaporation due to exfoliation. The red squares show evaporation in the presence of a notch in the same temperature as the blue triangles. The notch causes the gel to exfoliate earlier in the drying process and increases the evaporation rate. The black and red solid lines represent the fitting results for T = 21 °C (exponential decay) and T = 45 °C (linear regression), respectively. (B) Derivatives of the curves in (A) showing the time dependence of the solvent evaporation rate, $dm(t)/dt$, for the three different scenarios. In the case of the notched sample (red curve), the evaporation rate is approximately uniform, suggesting that the evaporation rate can be manipulated by changing the initial geometry. Inset: Zoom-in plot of C *versus* t for an initial drying period and the kinks, marked by arrows, indicate the onset of layer exfoliation.

Since exfoliation exposes much more surface than available in the original solid, the rate of drying should change as it is ultimately controlled by the exposed surface. In Fig. 4, we show that the drying rate remains approximately uniform even as the drying front penetrates deeply into the bulk. This observation potentially offers a new controlled release mechanism from a shrinking gel.[41]

Materials and methods

Gel sample preparation

A soft, lightly cross-linked PDMS network (Sylgard 184, Dow Corning) swollen in a selective solvent was used as a model gel. A series of PDMS gels with different geometries (cylinder, hemisphere, and flat disk) were fabricated *via* replica molding using a 40 : 1 mass ratio of prepolymer to cross-linker that was

mixed and poured over silicone negative molds. The mixture was left at room temperature for several hours to allow trapped air bubbles to escape and then cured at 75 °C in an oven overnight. After cooling, the cross-linked PDMS was carefully extracted from the mold and the weight and dimensions were measured. Hexanes (Sigma-Aldrich) was chosen as a swelling solvent due to its high tendency to swell PDMS.[42] Fabricated PDMS was immersed in hexanes at room temperature for at least two days to reach an equilibrium state of swelling, and the dimensions of swollen PDMS gel were measured. For the cylindrical gel, the radius and length increased from $R_0 \approx 6$ mm to $R \approx 13$ mm and from $L_0 \approx 30$ mm to $L \approx 63$ mm, respectively, resulting in an equilibrated swelling ratio of $\lambda(=R/R_0) \approx 2.2$. Note that an almost identical swelling ratio was obtained for the hemispherical and flat gels. The elastic modulus of the cross-linked PDMS in the dry state was $E \approx 100$ kPa, which was measured by a rheometer (Anton Paar Physica MCR 501).

Temperature-controlled drying experiments

The drying behavior of swollen gels was studied in an experimental setup in which the drying temperature T was adjusted by varying the distance between the gel and an incandescent lamp (65 W) and the solvent content of the gel during drying was determined by measuring the difference of gel weight before and during drying. The change in gel weight $m(t)$ was recorded using a digital balance (AR1530, Ohaus Corp.; resolution = 0.001 g) until there was no apparent change in weight during drying (typically several hours to a day). Photographs and videos were taken with a digital camera (Lumix DMC-GF2, Panasonic) equipped with a zoom lens (Lumix G Vario 14–42 mm lens), and thickness measurements of exfoliated layers were obtained from the video-recorded images. Approximate values of strain gradient were determined by measuring the crack opening displacement at the sample surface and the crack depth just before the superficial layer of gel begins to peel off. The mesh sizes of the cross-linked gel were calculated using the measured room-temperature values of E and λ according to ref. 43. The effective poroelastic diffusivities of the gel D_p at different T were estimated from curve-fitting the experimental drying data (before exfoliation) shown in Fig. 2A to a stretched exponential function: $(m_0 - m(t))/(m_0 - m_\infty) = \exp[-(a_1^2 D_p t/R^2)^\beta]$, where a_1 (=2.405) is the first root of the zeroth Bessel function and β is an exponent equal or close to one.[44] The estimated values of D_p were 0.56, 0.73, 0.91, and 1.39×10^{-8} m^2 s^{-1} for T = 21, 34, 45, and 57 °C, respectively. Note that D_p measured at T = 21 °C is close to the room-temperature self-diffusivity of hexanes $D_s \approx 0.43 \times 10^{-8}$ m^2 s^{-1} (ref. 45), implying a diffusion-limited process.

Effects of the size and composition of the sample and the wind speed

In the experimental results shown in Fig. 2D, the initial radius of the cylindrical gel was varied through the use of different size of the mold, while keeping the radius:length ratio of 1 : 5. Drying experiments were conducted at drying air temperature of 45 °C. To assess the dependence on the sample composition (the mass ratio of prepolymer to cross-linker of the PDMS), cylindrical gels were prepared at three different mass ratios (40 : 1, 25 : 1, and 10 : 1) but the same initial dimensions and were swollen to equilibrium in hexanes. With decreasing the mass ratio (*i.e.*, increasing the cross-link density), there was a decrease in a dimensional change of the gel upon swelling; the equilibrated swelling ratio for 25 : 1 and 10 : 1 gels was about 1.7 and 1.3, respectively. Drying experiments on these samples showed that the 25 : 1 gel is similar in fracture mode to the 40 : 1 gel (*i.e.*, spontaneous exfoliation), while the 10 : 1 gel exhibited bulk cracking without peeling. It is known that the speed of wind affects the evaporation rate. In some experiments, we subjected the samples to a constant wind forcing using an electronic fan. Wind speed was controlled by placing the fan at different distances from the sample and measured using a digital anemometer (SA-7, Sperry). The results of these experiments are presented in Fig. S4, ESI.†

Numerical simulations

The mass of the particles m, typical interaction distance σ, and typical interaction energy ε were used to define the following reduced units: the times t and τ were scaled by $(m\sigma^2/\varepsilon)^{1/2}$; coordinates $\mathbf{r}_i$, spring length d_{ij} and d_w, radius R, and front width w by σ; front velocity v_f by $(\varepsilon/m)^{1/2}$; fracture toughness Γ and Γ_w and spring constant $\mathscr{K}$ by ε/σ^2; friction coefficient ξ by $(\varepsilon m/\sigma^2)^{1/2}$. Fracture failures caused by drying shrinkage were simulated using a two-dimensional circular network made from a hexagonal lattice of point masses connected by elastic springs, which was subject to strain and/or fracture toughness gradients. A notch was added by cutting a few springs in the radial direction at an angle of $\pi/2$. For the simulation results, $d_w = 1$, $\Gamma_w = 2.55$, $\alpha_0 = 0.025$, $\tau = 6.5$, $R = 85$, $v_f = 0.01$, $\xi = 0.95$, and $\mathscr{K} = 50$. Images of the simulations in Fig. 3A–C were taken at t = 180, 180, and 1620, respectively.

Acknowledgements

We thank the Harvard MRSEC DMR 14-20570, the Wyss Institute for Biologically Inspired Engineering (J. Y. C. and L. M.) and the MacArthur Foundation (L. M.) for partial financial support.

References

1 E. M. Kindle, Some factors affecting the development of mud-cracks, *J. Geol.*, 1917, **25**(2), 135–144.
2 P. H. Morris, J. Graham and D. J. Williams, Cracking in drying soils, *Can. Geotech. J.*, 1992, **29**(2), 263–277.
3 S. Achanta, M. R. Okos, J. H. Cushman and D. P. Kessler, Moisture transport in shrinking gels during saturated drying, *AIChE J.*, 1997, **43**(8), 2112–2122.
4 C. J. Brinker and G. W. Scherer, *Sol-Gel Science: The Physics and Chemistry of Sol-Gel Processing*, Academic Press, 1990.
5 E. Reyssat and L. Mahadevan, Hygromorphs: from pine cones to biomimetic bilayers, *J. R. Soc., Interface*, 2009, **6**(39), 951–957.
6 S. Keck, Mechanical alteration of the paint film, *Stud. Conserv.*, 1969, **14**(1), 9–30.

7 G. W. Scherer, Theory of drying, *J. Am. Ceram. Soc.*, 1990, **73**(1), 3–14.
8 K. A. Shorlin, J. R. de Bruyn, M. Graham and S. W. Morris, Development and geometry of isotropic and directional shrinkage-crack patterns, *Phys. Rev. E: Stat. Phys., Plasmas, Fluids, Relat. Interdiscip. Top.*, 2000, **61**(6), 6950–6957.
9 L. Pel, K. A. Landman and E. F. Kaasschieter, Analytic solution for the non-linear drying problem, *Int. J. Heat Mass Transfer*, 2002, **45**(15), 3173–3180.
10 P. Lehmann, S. Assouline and D. Or, Characteristic lengths affecting evaporative drying of porous media, *Phys. Rev. E: Stat., Nonlinear, Soft Matter Phys.*, 2008, **77**, 056309.
11 L. Goehring, L. Mahadevan and S. W. Morris, Nonequilibrium scale selection mechanism for columnar jointing, *Proc. Natl. Acad. Sci. U. S. A.*, 2009, **106**(2), 387–392.
12 A. Groisman and E. Kaplan, An experimental study of cracking induced by desiccation, *EPL*, 1994, **25**(6), 415–420.
13 C. Allain and L. Limat, Regular patterns of cracks formed by directional drying of a colloidal suspension, *Phys. Rev. Lett.*, 1995, **74**(15), 2981–2984.
14 E. R. Dufresne, D. J. Stark, N. A. Greenblatt, J. X. Cheng, J. W. Hutchinson, L. Mahadevan and D. A. Weitz, Dynamics of fracture in drying suspensions, *Langmuir*, 2006, **22**(17), 7144–7147.
15 L. Goehring, Drying and cracking mechanisms in a starch slurry, *Phys. Rev. E: Stat., Nonlinear, Soft Matter Phys.*, 2009, **80**(3), 036116.
16 F. Giorgiutti-Dauphine and L. Pauchard, Elapsed time for crack formation during drying, *Eur. Phys. J. E: Soft Matter Biol. Phys.*, 2014, **37**, 39.
17 E. S. Matsuo and T. Tanaka, Patterns in shrinking gels, *Nature*, 1992, **358**, 482–485.
18 N. Tsapis, E. R. Dufresne, S. S. Sinha, C. S. Riera, J. W. Hutchinson, L. Mahadevan and D. A. Weitz, Onset of buckling in drying droplets of colloidal suspensions, *Phys. Rev. Lett.*, 2005, **94**(1), 018302.
19 K. Huraux, T. Narita, B. Bresson, C. Fretigny and F. Lequeux, Wrinkling of a nanometric glassy skin/crust induced by drying in poly(vinyl alcohol) gels, *Soft Matter*, 2012, **8**(31), 8075–8081.
20 W. H. Bradley, Factors that determine the curvature of mud-cracked layers, *Am. J. Sci.*, 1933, **26**(151), 55–71.
21 J. R. L. Allen, On the curl of desiccation polygons, *Sediment. Geol.*, 1986, **46**(1-2), 23–31.
22 D. Kovar, M. D. Thouless and J. W. Halloran, Crack deflection and propagation in layered silicon nitride/boron nitride ceramics, *J. Am. Ceram. Soc.*, 1998, **81**(4), 1004–1012.
23 S. Hillier, E. M. M. Marwa and C. M. Rice, On the mechanism of exfoliation of 'Vermiculite', *Clay Miner.*, 2013, **48**(4), 563–582.
24 P. W. Style, S. S. L. Peppin and A. C. F. Cocks, Mud peeling and horizontal crack formation in drying clays, *J. Geophys. Res.*, 2011, **116**(F1), F01025.
25 J. W. Hutchinson and Z. Suo, Mixed mode cracking in layered materials, *Adv. Appl. Mech.*, 1991, **29**, 63–191.
26 E. Reyssat and L. Mahadevan, How wet paper curls, *EPL*, 2011, **93**(5), 54001.
27 S. Douezan, M. Wyart, F. Brochard-Wyart and D. Cuvelier, Curling instability induced by swelling, *Soft Matter*, 2011, **7**(4), 1506–1511.
28 J. Y. Chung, K. Hunter and L. Mahadevan, Evaporative microclimate driven hygrometers and hygromotors, *EPL*, 2014, **107**(6), 64002.
29 T. Mizuguchi, A. Nishimoto, S. Kitsunezaki, Y. Yamazaki and I. Aoki, Directional crack propagation of granular water systems, *Phys. Rev. E: Stat., Nonlinear, Soft Matter Phys.*, 2005, **71**(5), 056122.
30 V. T. Karathanos and G. D. Saravacos, Porosity and pore size distribution of starch materials, *J. Food Eng.*, 1993, **18**(3), 259–280.
31 J. Zhang, Y. An, K. Yazzie, N. Chawla and H. Jiang, Finite element simulation of swelling-induced crack healing in gels, *Soft Matter*, 2012, **8**(31), 8107–8112.
32 X. Wang and W. Hong, Delayed fracture in gels, *Soft Matter*, 2012, **8**(31), 8171–8178.
33 T. M. Shaw, Drying as an immiscible displacement process with fluid counterflow, *Phys. Rev. Lett.*, 1987, **59**(15), 1671–1674.
34 I. N. Tsimpanogiannis, Y. C. Yortsos, S. Poulou, N. Kanellopoulos and A. K. Stubos, Scaling theory of drying in porous media, *Phys. Rev. E: Stat. Phys., Plasmas, Fluids, Relat. Interdiscip. Top.*, 1999, **59**(4), 4353–4365.
35 E. K. Rodriguez, A. Hoger and A. D. McCulloch, Stress-dependent finite growth in soft elastic tissues, *J. Biomech.*, 1994, **27**(4), 455–467.
36 K. A. Mazich and M. A. Samus, Role of entanglement couplings in threshold fracture of a rubber network, *Macromolecules*, 1990, **23**(9), 2478–2483.
37 K. A. Mazich, M. A. Samus, C. A. Smith and G. Rossi, Threshold fracture of lightly cross-linked networks, *Macromolecules*, 1991, **24**(10), 2766–2769.
38 A. Yuse and M. Sano, Transition between crack patterns in quenched glass plates, *Nature*, 1993, **362**(6418), 329–331.
39 P. G. de Gennes, Solvent evaporation of spin cast films: "crust" effects, *Eur. Phys. J. E: Soft Matter Biol. Phys.*, 2002, **7**(1), 31–34.
40 A. G. Evans and J. W. Hutchinson, The mechanics of coating delamination in thermal gradients, *Surf. Coat. Technol.*, 2007, **201**(18), 7905–7916.
41 J. Wang, J. A. Kaplan, Y. L. Colson and M. W. Grinstaff, Stretch-induced drug delivery from superhydrophobic polymer composites: use of crack propagation failure modes for controlling release rates, *Angew. Chem.*, 2016, **128**(8), 2846–2850.
42 J. N. Lee, C. Park and G. M. Whitesides, Solvent compatibility of poly(dimethylsiloxane)-based microfluidic devices, *Anal. Chem.*, 2003, **75**(23), 6544–6554.
43 Y. Hu, X. Chen, G. M. Whitesides, J. J. Vlassak and Z. Suo, Indentation of polydimethylsiloxane submerged in organic solvents, *J. Mater. Res.*, 2011, **26**(6), 785–795.
44 J. Crank, *The Mathematics of Diffusion*, Clarendon Press, 1975.
45 M. Holz and H. Weingartner, Calibration in accurate spin-echo self-diffusion measurements using ^{1}H and less-common nuclei, *J. Magn. Reson.*, 1991, **92**(1), 115–125.

